Distinct roles of cyclones and anticyclones in setting the midwinter minimum of the North Pacific eddy activity. Part II: Eulerian eddy statistics and energetics

Satoru Okajima,[a] Hisashi Nakamura,[a] Yohai Kaspi,[b]

[a] *Research Center for Advanced Science and Technology, The University of Tokyo, Tokyo, Japan*

[b] *Department of Earth and Planetary Sciences, Weizmann Institute of Science, Rehovot, Israel*

Corresponding author: Satoru Okajima, okajima@atmos.rcast.u-tokyo.ac.jp

ABSTRACT

The characteristics and dynamics of midlatitude storm-tracks have been long investigated. Nevertheless, our understandings of the storm-tracks, especially the midwinter minimum of the North Pacific storm-track activity, are still limited, partly because Eulerian eddy statistics are incapable of separating cyclonic and anticyclonic contributions. Here we investigate the detailed seasonal evolution of the contributions from cyclonic and anticyclonic vortices, identified with local wind curvature, to the Eulerian eddy statistics, eddy feedback forcing onto the climatological-mean westerly jet, and the energetics associated with the North Pacific storm-track. We demonstrate that the midwinter minimum of the net energy conversion/generation rate normalized by the eddy total energy over the entire North Pacific is more distinct for anticyclonic vortices than for cyclonic vortices, to which the midwinter minimum of the probability of anticyclonic vortices contributes. The main factors include the reduction of the baroclinic energy conversion into midwinter and the reduction of the net energy outflux into spring. To long-term modulations of the MWM of the NP storm-track activity, both cyclonic and anticyclonic vortices contribute constructively. Together with our companion paper, the present study reveals the primal importance of migratory anticyclones for the midwinter minimum of the North Pacific storm-track activity. We posit a viewpoint of considering roles of both migratory cyclones and anticyclones for the storm-track dynamics, the latter of which has been long disregarded unconsciously.

1. Introduction

Midlatitude transient eddies that give rise to day-to-day weather variability are one of the rudimentary components of the Earth's climate system. Those migratory cyclones and anticyclones interact with climatological-mean states and low-frequency, quasi-stationary anomalies in which they are embedded. Passing over a given midlatitude location recurrently, they locally account for a major fraction of high-frequency sub-weekly fluctuations of a given atmospheric variable. Landsberg et al. (1959) found a variability whose period is between 5-7 days on top of that of 15-25 days from a station temperature data. Based on a 10-year atmospheric analysis data over the entire extratropical Northern Hemisphere, Blackmon (1976) decomposed the variance of 500-hPa height into high-pass, band-pass (with periods of 2−6 days), and low-pass filtered components. His result suggested that regions of large band-pass variance correspond to those of frequent cyclone passage over the North Atlantic (NA) and North Pacific (NP) basins. Blackmon et al. (1977) further pointed out that those regions are characterized by prominent poleward eddy heat flux based on the band-pass-filtered fluctuations in temperature and meridional wind velocity at 850-hPa, referring to them as "storm-tracks". A zonally-elongated region of pronounced poleward heat transport associated with sub-weekly transient eddies, a measure of their baroclinic development, is also found located over the South Indian Ocean (Nakamura and Shimpo 2004). Those three major storm-tracks are collocated with the lower-tropospheric eddy-driven westerly jets and associated lower-tropospheric baroclinic zones (Nakamura et al. 2004), and they are maintained under the effective restoration by major oceanic frontal zones (Hotta and Nakamura 2011).

The Eulerian statistics utilize gridded atmospheric data, including operational analysis and global reanalysis data, which have been available since the mid-1970s and mid-1990s, respectively. The Eulerian approach became common in the 1980s. Since then, climatological-mean seasonality, and interannual and decadal-scale variations have been investigated through Eulerian statistics (e.g., Chang et al. 2002). For Eulerian eddy statistics, temporal digital filters are commonly used to extract sub-weekly fluctuations associated with extratropical high-frequency, synoptic-scale disturbances. Eulerian statistics are compatible with the quantitative analyses and dynamical diagnostics, including the "Lorenz energy cycle", in which exchanges are evaluated between kinetic and available potential energies and between the zonal-mean averaged and eddy components (Lorenz 1955). For example, the formation and maintenance mechanisms for the mean state and storm-track activity can be examined through energy budget analysis (e.g., Orlanski and Katzfey 1991; Chang et al. 2002). The (extended) Eliassen-Palm (E-P) flux, which represents the propagation of Rossby wave packets and associated translation of wave-activity pseudo-momentum, is useful for assessing the wave-mean flow interaction (Hoskins et al. 1983; Trenberth 1986; Plumb 1986).

Expanding Lee and Kim (2003), Nakamura et al. (2004) illustrated the maintenance mechanisms for the westerly jets and storm-tracks, with particular emphasis on the lower-boundary condition. They contrasted a regime characterized by a well-defined eddy-driven subpolar jet separated from a subtropical jet with another regime by a stronger subtropical jet. In the former regime, a storm-track and an associated eddy-driven westerly jet extend from the surface to the upper troposphere, anchored along a subarctic oceanic frontal zone, as typically observed in the summertime Southern Hemisphere, the NP shoulder seasons (autumn and spring) and the NA. Transient eddies systematically transport westerly momentum poleward and downward from a subtropical jet to maintain the deep eddy-driven jet. In the latter regime, as typically observed in the wintertime Southern Hemisphere, the upper-tropospheric storm-track is trapped into the subtropical jet core, while the low-level storm-track forms along an oceanic frontal zone. They argued that the midwinter NP is in-between, characterized by a hybrid jet through a merger of subpolar and subtropical jets.

Nakamura (1992) found that the NP storm-track activity, measured by RMS of the band-pass filtered upper-tropospheric geopotential height fluctuations, exhibits a clear minimum in midwinter. It is inconsistent with the baroclinic instability theory (Eady 1949), in which the maximum growth rate of eddies is proportional to the vertical shear of the zonal winds, given that the westerly jet speed over the NP is clearly maximized in midwinter. It is in sharp contrast to the midwinter maximum of the NA storm-track activity, which is compatible with the theory. This counterintuitive phenomenon has been referred to as “midwinter minimum (MWM)” or “midwinter suppression” of the NP storm-track activity, for which multiple mechanisms have been proposed. They include barotropic and baroclinic aspects of eddies, diabatic heating, an upstream influence (or seeding effect), and structures of the jet streams (see literatures in Okajima et al. 2022a; hereafter referred to as Part I). To date, however, no single mechanism has been proposed that can explain the existence of the MWM of the NP storm-track activity.

For a quantitative comparison among the proposed mechanisms, energy budget analysis is a powerful tool. Zhao and Liang (2019) examined the energetics of migratory eddies along the NP storm-track in relation to its MWM. However, they evaluated only energy conversion/generation rates, which is inevitably dependent of eddy amplitude. Their findings are therefore insufficient for full consideration of the mechanisms for the suppressed eddy activity. Chang (2001) defined “growth rates” as the local eddy energy conversion/generation rates for the NP storm-track divided by local eddy kinetic energy (EKE). The normalization by local EKE is, however, debatable from the basin-scale characteristic of the NP storm-track with obvious downstream translation of eddy energy. Schemm and Rivière (2019) evaluated “efficiency” of some of the energetic terms, which is independent of eddy amplitude, but their analysis is rather limited to particular pressure levels and variables. It is therefore necessary to perform more comprehensive energetics of eddies along the NP storm-track for clarifying the mechanisms for the MWM. More recently, Okajima et al. (2022; hereafter ONK22) comprehensively evaluated the detailed seasonal evolution of energy conversion/generation rates associated with transient eddies along the NP storm-track, normalized by the eddy total energy. Giving a perspective of the MWM of the NP storm-track activity that encompasses various mechanisms proposed by previous studies, they found that the net normalized energy conversion/generation rate is indeed suppressed in midwinter. Their results demonstrated that conversion of available potential energy (APE) from the climatological-mean state to eddies plays a substantial role especially in the reduction of the normalized total energy conversion/generation rate in midwinter from its early-winter peak, whereas that of the energy influx from the upstream is particularly important for the spring recovery.

Over decades, considerable effort has been devoted to investigating the characteristics and dynamics of midlatitude storm-tracks. Nevertheless, our understandings of storm-tracks are still limited, including the MWM of the NO storm-track activity. One of the reasons is that Eulerian statistics, which facilitate a quantitative diagnosis and analysis, assumes linearity of eddy-associated fluctuations and therefore cannot handle cyclones and anticyclones separately. Lagrangian tracking, by contrast, enables to analyze them separately but is not suited for a quantitative analysis, especially for eddy-mean flow interactions. These two methods are intrinsically complementary, but they have been applied separately in most of the previous studies. Some studies conducted analyses of both Eulerian statistics and Lagrangian tracking, but just in parallel (Chang et al. 2002; Hoskins et al. 2019a, b). In fact, a region of pronounced high-frequency SLP variance in the Eulerian framework does not necessarily coincide with a region of frequent cyclone tracks in the Lagrangian framework. Wallace et al. (1988) documented the behavior of high-frequency fluctuations in geopotential height, to reveal that cyclones tend to move northeastward to the east of Japan, not along the zonally-elongated "storm-track" identified by Blackmon (1976). Comparison between Eulerian variance and feature-tracking statistics by Penny et al. (2010) was immensely simplified, assuming eddies as a series of identical non-overlapping sine-shaped pulses. Schemm and Rivière (2019) attempted to evaluate the APE conversion only around surface cyclones by accumulating the local APE conversion within circles of a given threshold radius centered at a cyclone center, or the outermost closed SLP contour. Nevertheless, surface cyclones and associated cyclonic vortices are neither circular nor vertical. Additionally, they did not assess the contribution from anticyclones.

Recently, Okajima et al. (2021; hereafter ONK21) proposed a novel method to identify three-dimensional domains of individual cyclonic and anticyclonic vortices based on local curvature, and to evaluate separate contributions from cyclonic and anticyclonic vortices to Eulerian eddy statistics and atmospheric energetics. Local curvature and related quantities have been utilized for tracking mid- to upper-tropospheric troughs (Lefevre and Nielsen-Gammon 1995; Schemm et al. 2020), but they have not been used to separate and reconstruct eddy Eulerian statistics. Combined with the framework for the comprehensive energetics of storm-tracks independent of the eddy amplitude by ONK22, the "hybrid perspective" method will effectively illustrate the seasonal evolution of the separate contributions from cyclonic and anticyclonic vortices to the Eulerian eddy statistics and atmospheric energetics.

The present study thus aims to investigate the detailed seasonal evolution of the separate contributions from cyclonic and anticyclonic vortices to Eulerian eddy statistics, eddy feedback forcing onto the climatological-mean westerly jet, and energetics associated with the NP storm-track. In Part I, seasonal evolution of the frequency of surface cyclones and anticyclones are investigated based on a Lagrangian tracking, focusing especially on the importance of anticyclones traveling from the Japan Sea into the NP.

This paper (Part II) continues in section 2 with a description of data used and analysis methods. Sections 3 and 4 delineate seasonality of cyclonic and anticyclonic contributions to eddy Eulerian statistics and eddy feedback forcing on the background westerlies. Section 5 investigates separated energetics for the NP storm-track. Section 6 describes the long-term modulations in the energetics briefly. Section 7 offers a summary and discussions.

2. Data and analysis methods

a. observational data

Same as in Part I, this study utilizes atmospheric variables, including geopotential height, temperature, wind velocities, and diabatic heating rates in pressure coordinates as well as sea-level pressure (SLP), from the Japanese 55-year reanalysis (JRA-55; Kobayashi et al. 2015; Harada et al. 2016) for the period 1958-2017. Those variables are available on a 1.25°×1.25° grid.

At each grid point, fluctuations of a given variable with synoptic-scale transient eddies have been extracted from the 6-hourly atmospheric reanalysis as its deviations from their low-pass-filtered fields through a Lanczos filter with a 121-point window and a cutoff period of 8 days. Climatological-mean fields are calculated from 31-day running mean fields.

b. Separation of cyclonic and anticyclonic contributions to eddy Eulerian statistics

Following the methodology developed by ONK21, climatological-mean eddy Eulerian statistics are calculated separately for cyclonic and anticyclonic contributions. Local curvature κ_2 is calculated at a given vertical level instantaneously from zonal and meridional winds (u, v) as

$$\kappa_2 \equiv \frac{1}{R_S} = \frac{1}{V^3}\left(-uvu_x + u^2 v_x - v^2 u_y + uvv_y\right), \qquad (1)$$

where R_S denotes the curvature radius, V scaler wind speed and a subscript zonal or meridional derivative. This can be derived also from the definition of two-dimensional curvature with an implicit curve of geostrophic streamfunction (Goldman 2005). Note that this method does not require any temporal filtering to determine the shape of vortices, and therefore near-surface curvature corresponds directly to counterclockwise (clockwise) rotations associated with a cyclone (anticyclone) over the NH.

Separate contributions from cyclonic and anticyclonic vortices (or eddies) to Eulerian statistics is evaluated by accumulating instantaneous contributions only at grid points where cyclonic or anticyclonic curvature is observed. In the following, the threshold curvature for cyclonic and anticyclonic rotations are set to be zero so as not to miss any circulation on the fringe of pressure troughs and ridges, unless otherwise specified. Note that the conclusions are qualitatively similar with the requirement for vortices to accompany corresponding surface features (see Appendix).

c. Energetics

The framework of the energetics for transient eddies along storm-tracks basically follows ONK22. Climatological-mean eddy APE (EAPE) and eddy kinetic energy (EKE) associated with sub-weekly disturbances are defined as:

$$\mathrm{EAPE} = \frac{R}{p\mathrm{S_p}}\left(\frac{(T'^2)_C}{2}\right), \mathrm{EKE} = \frac{(u'^2+v'^2)_C}{2}, \tag{2}$$

where primes denote sub-weekly fluctuations, subscripts "*c*" the climatological-mean fields, and $\mathrm{S_p}$ $(\equiv -\overline{T_c}\,\partial\ln\overline{\theta_c}/\partial p)$ a stability parameter. Overbars denote horizontally-averaged quantities over a specific domain. In (2), *u, v, T*, and *R* represent zonal and meridional wind components, temperature, and the gas constant for dry air, respectively.

Energy conversion/generation rates are defined as in (3), assuming quasi-geostrophic scaling. Additionally, time tendency of horizontally-averaged climatological-mean static stability is omitted. In the following, *CK* denotes the barotropic energy conversion (or KE conversion), *CP* the baroclinic energy conversion (or APE conversion), and *CQ* the APE generation through diabatic processes:

$$CK = \frac{(v'^2-u'^2)_C}{2}\left(\frac{du_c}{dx}-\frac{dv_c}{dy}\right) - (u'v')_C\left(\frac{du_c}{dy}+\frac{dv_c}{dx}\right) \tag{3a}$$

$$CP = \frac{R}{p\mathrm{S_p}}\left(-(u'T')_C\frac{dT_c}{dx} - (v'T')_C\frac{dT_c}{dy}\right) \tag{3b}$$

$$CQ = \frac{R}{p\mathrm{S_p}}(Q'T')_C \tag{3c}$$

$$ET = -\frac{R}{p}(\omega'T')_C, \tag{3d}$$

where *Q* signifies temperature tendency due to diabatic processes and *ω* pressure velocity.

In this study, the energy conversion/generation terms are integrated vertically from the surface to the 100-hPa level and then integrated horizontally over the NP domain [130°E−130°W, 20−65°N]. Energy influx or outflux through the lateral boundaries of the domain (EF) needs to be evaluated for the energetics within the domain. The flux can be expressed as:

$$EF = \int_{p_s}^{p_{\mathrm{top}}} \{(\Phi'\mathbf{v}')_C + (\mathrm{EAPE} + \mathrm{EKE})\mathbf{v}_c\}\ dp, \tag{4}$$

where Φ is geopotential, p_s denotes surface pressure, and p_{top} is set to be 100 hPa.

As in ONK22, the "normalized rate" of each of the energy conversion, generation and flux terms is evaluated by dividing the term by the total eddy energy defined as the sum of EAPE and EKE:

$$\text{Normalized rate} \equiv \frac{\text{<Energy conversion/generation term>}}{\text{<EAPE+EKE>}}. \tag{5}$$

This "normalized rate of conversion (or generation)" represents a replenishing rate in unit of [day^{-1}], and its reciprocal thus gives a time scale of how long it would take to replenish the total eddy energy within the storm-track domain solely by a given conversion/generation process. Hereafter, to improve visibility, we refer to the normalized rate simply as "λ" and a subscript as listed in Table 1 is added in referring to a specific conversion/generation process as in ONK22[1]. Because the energy conversion/generation rate, by definition, depends on eddy amplitude, it is essential for the energetics to evaluate it as its normalized rate, which is independent of eddy amplitude. In our definition negative values of λ mean that eddies are giving up energy to the time-mean circulation.

Symbol	Meaning
$\boldsymbol{\lambda_{CK}}$	Rate of CK (barotropic energy conversion) normalized by (EKE+EAPE)
$\boldsymbol{\lambda_{CP}}$	Rate of CP (baroclinic energy conversion) normalized by (EKE+EAPE)
$\boldsymbol{\lambda_{CQ}}$	Rate of CQ (diabatic energy generation) normalized by (EKE+EAPE)
$\boldsymbol{\lambda_{EF}}$	Rate of EF (net energy influx/outflux) normalized by (EKE+EAPE)

[1] We also calculate barotropic and baroclinic energy conversion rates from low-frequency variability to sub-weekly eddies ("LF" terms in ONK22). It was found to be relatively small and thus omitted in the present study.

$\boldsymbol{\lambda_{Tot}}$	Rate of total energy conversion/generation rate (sum of the above terms) normalized by (EKE+EAPE)
$\boldsymbol{\lambda_{ET}}$	Rate of ET (energy transfer from EKE to EAPE) normalized by (EKE+EAPE)

Table 1. List of the symbols for the normalized rates used in this study. All quantities are expressed in the unit of [day^{-1}].

3. Cyclonic and anticyclonic contributions to Eulerian statistics and their seasonality

First, we examine the seasonal evolution of climatological-mean probability distributions of cyclonic and anticyclonic vortices over the NP (Fig. 1). The three calendar days indicated in Fig. 1 correspond to the first peak, MWM and second peak of the NP storm-track activity (Nakamura 1992; ONK22). As pointed out by ONK21, probability of upper-level cyclonic vortices is higher poleward of the jet axis in midwinter and vice versa for anticyclonic vortices (Fig. 1b). This may be attributed to the effect of “trough thinning and broadening” by meridional shear of the jet (Thorncroft et al. 1993), given that those vortices are identified by local curvature free from shear vorticity. As shown in Fig. 1e, probability of lower-tropospheric cyclonic vortices (and anticyclonic counterpart as the local residual) is consistent with the result by feature tracking at the surface (Part I). In the shoulder seasons, the upper- and lower-tropospheric probability distributions of vortices basically follow the poleward displacement of the westerly jet as its seasonal evolution (Fig. 1). Midwinter equatorward expansion of high probability of cyclonic vortices, equivalently equatorward retreat of a domain of frequent anticyclonic vortices, also corresponds to those of surface migratory cyclones and anticyclones, the latter of which is largely regulated by anticyclones from the Japan Sea (Part I).

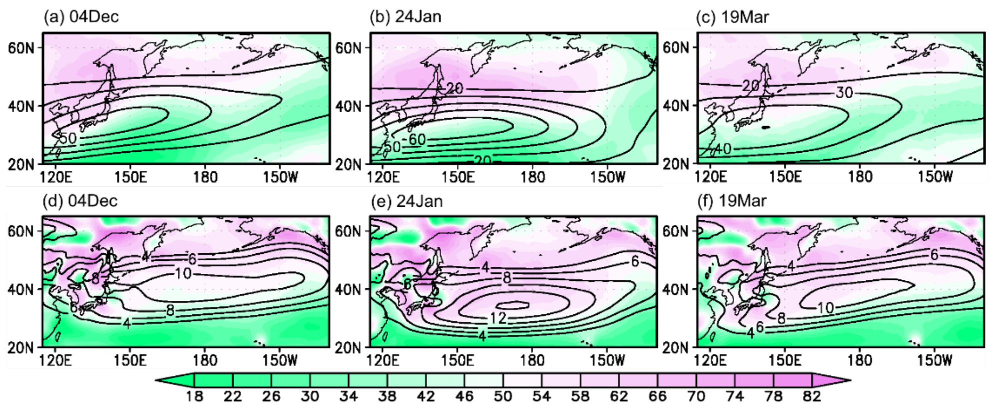

Fig. 1. Climatological probability distributions of cyclonic vortices (colors; with positive curvature) at the (a-c) 300-hPa and (d-f) 850-hPa levels, for the indicated calendar days as indicated. The probability of anticyclonic vortices can be obtained as the local residual. Black contours indicate climatological-mean (a-c) U_{300} and (d-f) U_{850} (m/s).

Figure 2 shows climatological-mean distributions of the variance of sub-weekly fluctuations of 300-hPa meridional wind ($V'V'_{300}$) evaluated as the separate contributions from cyclonic and anticyclonic vortices. For both polarities, $V'V'_{300}$ maximizes in the eastern NP as in the total variance (black contours in Fig. 2). While the maximum value of the cyclonic $V'V'_{300}$ remains largely unchanged from early winter into spring (Figs. 2a-c), anticyclonic $V'V'_{300}$ exhibits its distinct MWM. It is stronger than its cyclonic counterpart in the shoulder seasons especially over the central and eastern NP (Figs. 2d-f). These characteristics are clearly seen in latitude-season sections (Figs. 2g-h), indicative of the primary importance of anticyclonic vortices for the distinct MWM between the dual peaks in the climatological-mean $V'V'_{300}$.

Conversely, cyclonic $V'V'_{850}$ is much stronger than its anticyclonic counterpart (Figs. 2i-j), with their maxima located over the western NP (ONK22). The stronger wind fluctuations associated with lower-tropospheric cyclonic vortices are congruous with our perception of migratory cyclones as “storms”. The contribution from cyclonic vortices to $V'V'_{850}$ is nearly constant, and the peak latitude largely coincides with the climatological axis of $V'V'_{850}$. By contrast throughout the cold season, its anticyclonic counterpart is stronger in early winter than in spring with a moderate MWM in between, and the peak latitude is displaced to the south of the climatological-mean axis of $V'V'_{850}$. The contribution of anticyclonic vortices to the MWM of the total $V'V'_{850}$ (black contours in Figs. 2i-j) is evident, though in smaller amplitude.

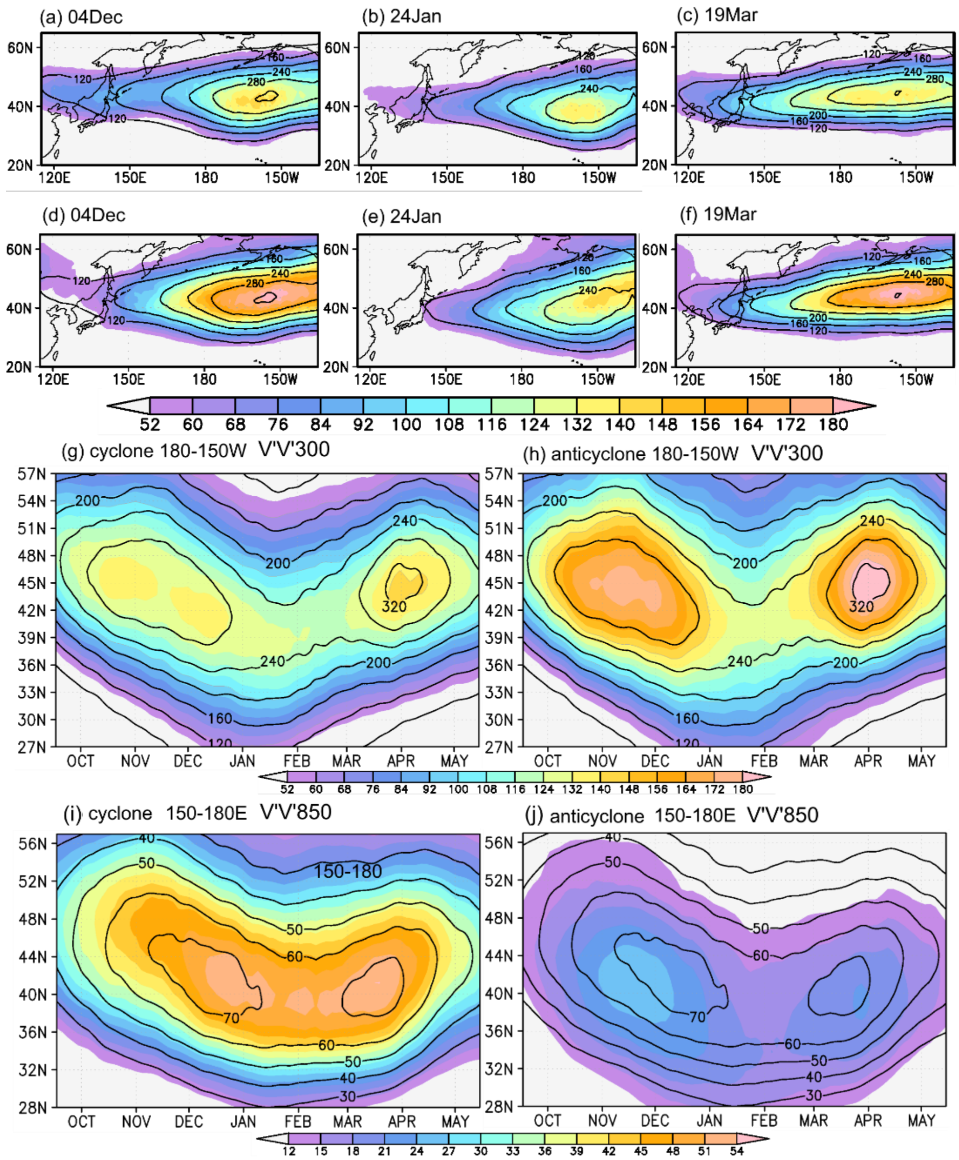

Fig. 2. (a-c) Climatological-mean distributions of $V'V'_{300}$ (color, m^2/s^2) for the calendar days as indicated, reconstructed only with cyclonic vortices. Contours denote climatological-mean total $V'V'_{300}$ from all vortices (m^2/s^2). (d-f) Same as in (a-c), respectively, but for anticyclonic vortices. (g) Climatological seasonality in $V'V'_{300}$ reconstructed only with cyclonic vortices averaged for 180°−150°W. Contours denote the corresponding seasonality of total $V'V'_{300}$ from all vortices. (h) Same as in (g), but for anticyclonic vortices. (i, j) Same as in (g, h), respectively, but for $V'V'_{850}$ averaged over 150°−180°E.

Similarly, lower-tropospheric poleward eddy heat flux ($V'T'_{850}$) associated with cyclonic vortices is much stronger than its anticyclonic counterpart (Fig. 3). The cyclonic contribution is found to maximize in spring with no apparent MWM (Figs. 3a-c). Though weaker in general, the anticyclonic contribution, by contrast, exhibits a distinct MWM between its primary early-winter peak and its secondary spring peak (Figs. 3d-f). These characteristics are more discernible in the latitude-season sections (Figs. 3g-h), indicative of the indispensable role of anticyclonic vortices in forming the MWM of the climatological-mean $V'T'_{850}$.

Related to this, seasonality of the upward component of the phase-independent wave-activity flux defined by Takaya and Nakamura (2001) differs between cyclonic and anticyclonic vortices, as shown in Fig. 4. This flux component is related to both the down-gradient eddy heat flux and background static stability. The lower-tropospheric upward wave-activity flux associated with cyclonic vortices exhibits its distinct midwinter maximum (Fig. 4b), which is contributed to mainly by the reduced static stability (not shown). Meanwhile, its anticyclonic counterpart maximizes in early winter and gradually weakens into spring (Figs. 4d-f). Just below the westerly jet core (~400 hPa), the upward wave-activity flux exhibits a MWM for both cyclonic and anticyclonic vortices. In the upper troposphere above the 400-hPa level, the upward component of the wave-activity flux diminishes, while its eastward component becomes dominant. Compared with its counterpart associated with cyclonic vortices, the eastward component associated with anticyclonic vortices is stronger and its maximum extends farther downstream into the eastern NP. Since the wave-activity flux plotted in Fig. 4 does not include the term as a product of the phase velocity and wave-activity pseudo-momentum associated with migratory eddies, our result is indicative of the greater contribution to the downstream development of transient eddies from anticyclonic vortices[2], and the contribution exhibits a MWM.

---

[2] Horizontal components of the wave-activity flux in this analysis should be interpreted with caution. The flux is evaluated for sub-weekly eddies, whereas the corresponding vortices are identified in unfiltered wind fields, from which the contribution from the NP westerly jet has been removed. Although those eddies and vortices are closely related to each other as seen in Fig. 1, the eastward wave-activity flux may not directly indicate downstream developing vortices.

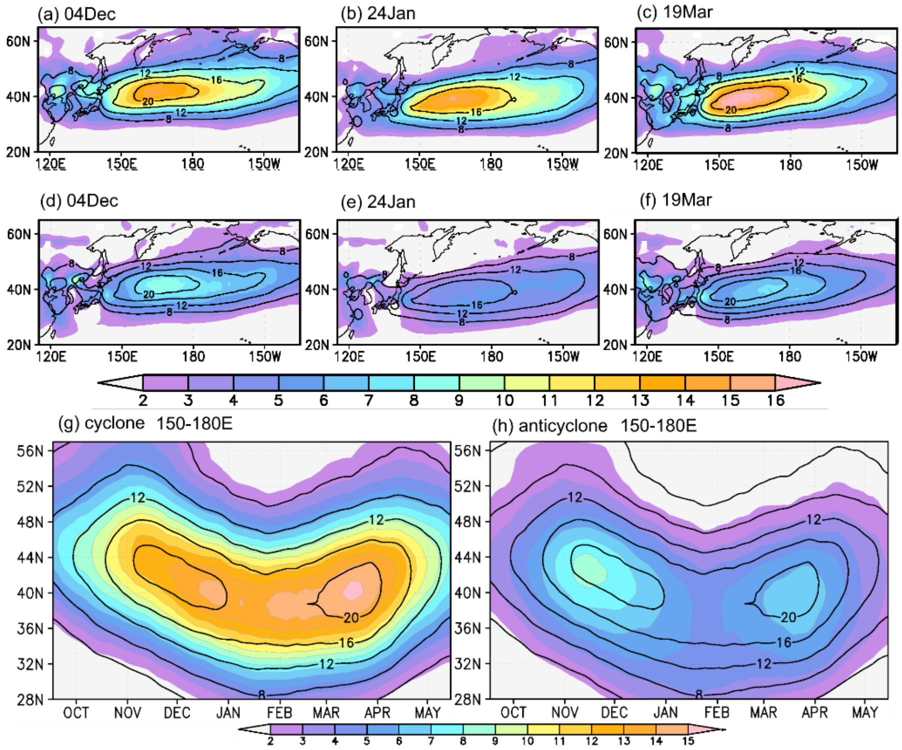

Fig. 3. (a-f) Same as in Figs. 2a-f, respectively, but for $V'T'_{850}$ (K m/s). (g, h) Same as in Figs. 2g-h, respectively, but for $V'T'_{850}$ (K m/s) averaged over 150°−180°E.

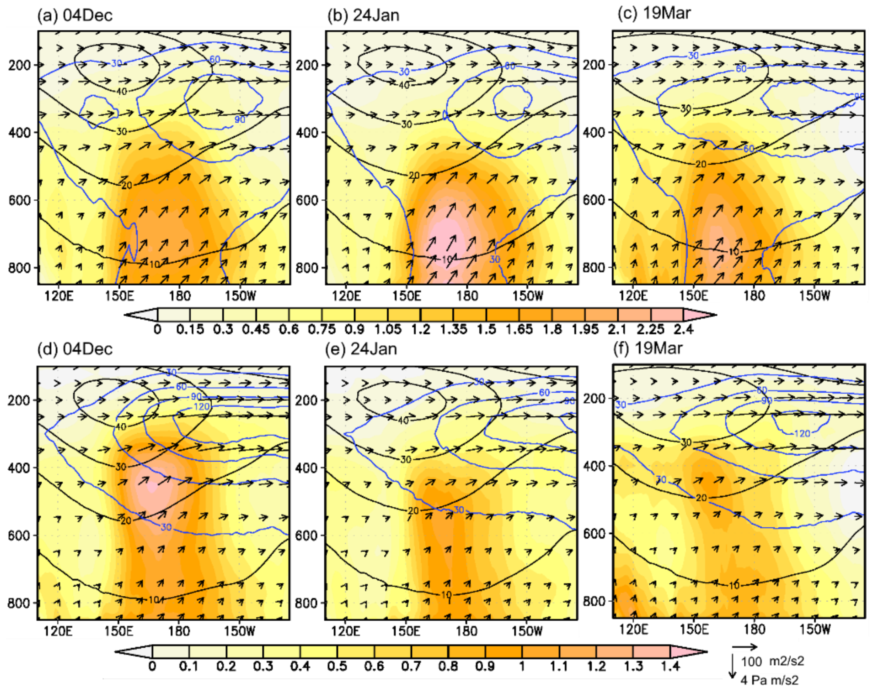

Fig. 4. (a-c) Zonal sections of climatological-mean wave-activity flux (vectors) formulated by Takaya and Nakamura (2001), which evaluated for sub-weekly disturbances but only from cyclonic vortices for (a) 04Dec, (b) 24Jan, and (c) 19Mar. The flux plotted here does not include the term as a product of the phase velocity and wave-activity pseudo-momentum associated with sub-weekly disturbances. Colors and blue contours indicate its upward (Pa m/s^2) and eastward (m^2/s^2) components, respectively. Black contours denote

climatological-mean westerly wind speed (m/s). Quantities shown are meridionally averaged in 30°−55°N. (d-f) Same as in (a-c), respectively, but for anticyclonic vortices.

To investigate westerly momentum transport by cyclonic and anticyclonic vortices, their contributions to $U'V'_{300}$ are shown in Fig. 5. The contributions from vortices of both polarities show a striking meridional contrast characterized by positive (negative) $U'V'$ to the south (north) of the climatological-mean NP westerly jet. Zero lines of $U'V'_{300}$ tend to be zonally oriented between ~40°N and 45°N, indicating that the westerly acceleration by both cyclonic and anticyclonic eddies occurs slightly to the north of the NP jet axis. Over East Asia, positive $U'V'_{300}$ is clearly shifted poleward of the primary jet axis in the subtropics without noticeable negative $U'V'_{300}$. Obviously, the amplitude of $U'V'_{300}$, especially its negative values north of the jet, is larger for the anticyclonic contribution even in midwinter, when the magnitude of anticyclonic $V'V'_{300}$ is comparable to its cyclonic counterpart (Fig. 2). Consistently, the negative U'–V' correlation to the north of the jet axis is more prominent for anticyclonic vortices, while the positive correlation is generally stronger for cyclonic vortices farther to the south of the jet axis (not shown). For both cyclonic and anticyclonic vortices, midwinter is the season when the negative correlation north of the jet is most prominent.

In the lower troposphere, by contrast, the contribution from cyclonic vortices to the meridional westerly momentum transport is much larger than that from anticyclonic vortices, especially on the northern flank of the jet (Fig. 6). This means that cyclonic vortices overall act to transport westerly momentum effectively into the lower-tropospheric eddy-driven jet from the Aleutian Low located to the north. Although lower-tropospheric cyclonic vortices contribute dominantly to the negative $U'V'$, the negative U'–V' correlation to the north of ~40°N is roughly comparable between cyclonic and anticyclonic vortices (not shown). The prominent negative lower-tropospheric $U'V'$ north of the low-level jet axis is a manifestation of the dominance of cyclonic vortices in sub-weekly wind fluctuations as shown in Figs. 2i-j.

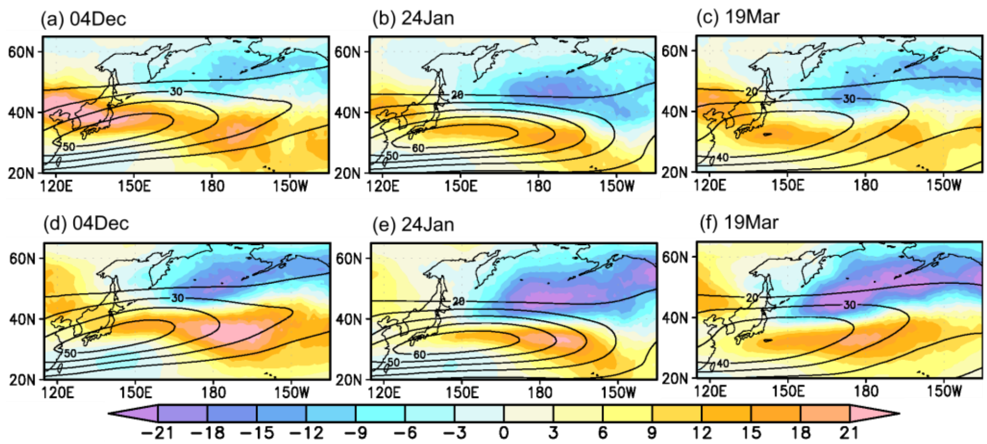

Fig. 5. Same as in Figs. 2a-f, respectively, but for $U'V'_{300}$ (m^2/s^2). Black contours denote climatological-mean U_{300} (m/s).

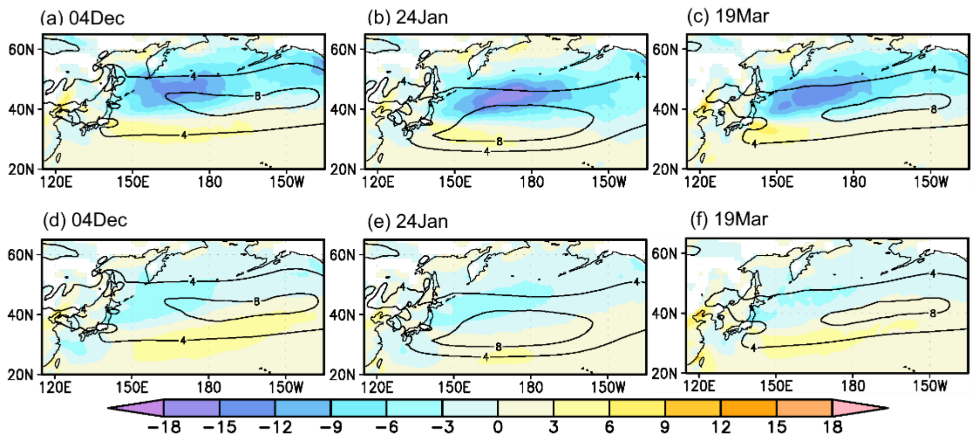

Fig. 6. Same as in Fig. 5, but for $U'V'_{925}$.

4. Cyclonic and anticyclonic contributions to eddy feedback forcing on the westerlies and their seasonality

The deformation of cyclonic and anticyclonic vortices implies that they act to yield a converging flux of westerly momentum into the jet as discussed in previous studies (e.g., Blackmon et al. 1977; Lau and Holopainen 1984; ONK21), and their seasonality can exert some influence onto the seasonal march of the NP westerly jet. To quantify the westerly acceleration or deceleration as the separate contributions from cyclonic and anticyclonic vortices, three-dimensional transient eddy feedback forcing onto background westerlies is calculated in following ONK22.

Figure 7 shows meridional sections of westerly wind acceleration/deceleration by eddy heat and vorticity fluxes over the western NP as separate contributions from cyclonic and anticyclonic vortices. In the cold season, both cyclonic and anticyclonic vortices act to reinforce the NP westerly jet slightly to the north of its axis. In the lower troposphere, the westerly acceleration centered at ~40°N by cyclonic vortices (Figs. 7a-c) is much stronger than that by anticyclonic vortices (Figs. 7d-f), consistently with the upward extended E-P flux (Fig. 7). The westerly deceleration north of ~50°N also arises mainly from cyclonic vortices, in agreement with $U'V'_{925}$ (Fig. 6). As pointed out by ONK21, the westerly acceleration by anticyclonic vortices is more coherent vertically (Figs. 7d-f), and it is comparable with or even stronger than that by cyclonic vortices in the upper troposphere. Correspondingly to the midwinter maximum of the equatorward transport of westerly momentum by cyclonic vortices to the north of the upper and lower-tropospheric jet axes (Figs. 5b and 6b), the westerly acceleration/deceleration by cyclonic vortices are strongest in midwinter, especially along ~40°N in the mid- and upper troposphere and ~50°N in the lower troposphere. Conversely, the lower-tropospheric westerly acceleration by anticyclonic vortices is somewhat suppressed in midwinter (Fig. 7e), consistent with the suppression of midwinter $V'T'_{850}$ (Fig. 3h).

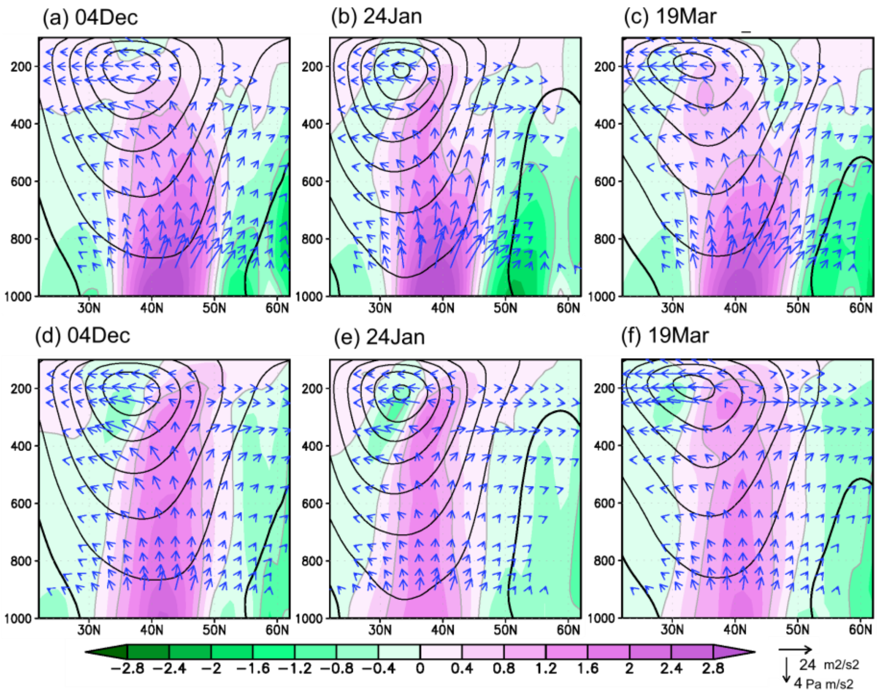

Fig. 7. (a-c) Meridional sections of climatological-mean net westerly wind acceleration or deceleration as transient eddy feedback forcing (color, m/s/day) by cyclonic vortices for the calendar days as indicated. All the quantities plotted are zonally averaged for 150°−180°E. Black contours denote climatological-mean westerly wind speed (every 10m/s, thick for 0 m/s). Vectors indicate the extended E-P flux associated with transient eddies. (d-f) Same as in (a-c), respectively, but for anticyclonic vortices.

The seasonal evolution of westerly wind acceleration/deceleration is highlighted in latitude-season sections in Fig. 8. Throughout the cold season, the upper-tropospheric westerly acceleration (deceleration) to the north (south) of the NP jet axis by anticyclonic vortices is stronger than its cyclonic counterpart. This is indicative of a more important role of anticyclonic vortices in transporting westerly momentum poleward from the NP hybrid jet, the equatorward portion of which is maintained thermally by the Hadley Cell. The predominance of the contribution from anticyclonic vortices to the westerly acceleration is slightly reduced in midwinter from the shoulder seasons, reflecting the midwinter maximum in the cyclonic contribution to $U'V'_{300}$ to the north of the jet axis (Fig. 8b). In the lower troposphere, westerly acceleration by cyclonic vortices remains rather constant throughout the cold season with the midwinter maximum of westerly deceleration to the north (Fig. 8c). The westerly acceleration by anticyclonic vortices, in contrast, exhibits its modest MWM with a noticeable peak in late autumn through early winter, which may be related to the early-winter peak of mid-tropospheric $V'T'$ (Fig. 4d). Interestingly, southward expansion of the near-surface westerly jet (~30°N) in midwinter is attributable only to the acceleration by anticyclonic vortices, counteracting the deceleration by cyclonic vortices in the subtropics.

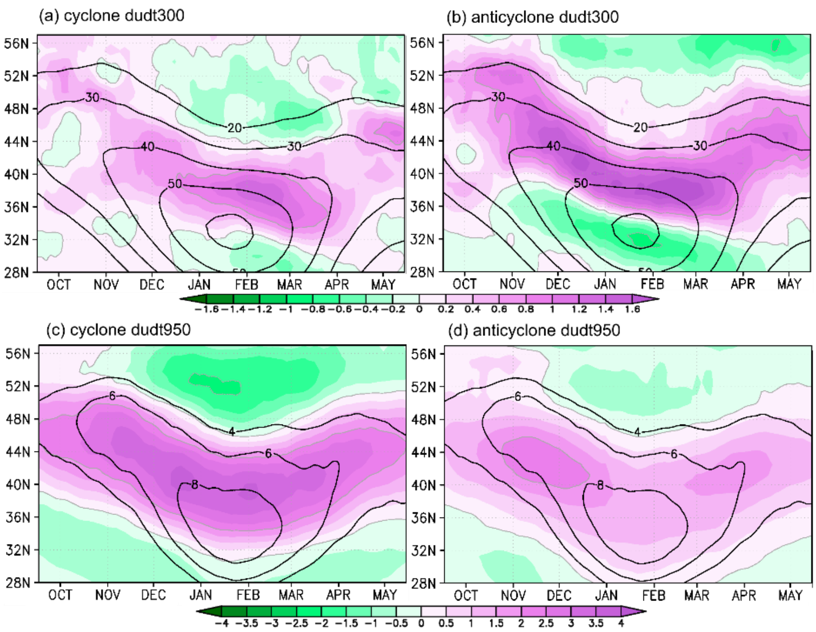

Fig. 8. (a) Climatological seasonality in net westerly wind acceleration or deceleration as transient eddy feedback forcing (color, m/s/day) at 300-hPa by cyclonic vortices. Black contours denote climatological-mean U_{300}. All the quantities plotted are averaged for 150°−180°E. (b) Same as in (a), but for anticyclonic vortices. (c, d) Same as in (a, b), respectively, but for the results at 950-hPa.

5. Separated energetics for the North Pacific storm-track

In this section, we evaluate the energetics for the NP storm-track based on the Eulerian statistics that are decomposed into contributions from cyclonic and anticyclonic vortices as in ONK21. Figures 9a and 9b show seasonal evolution of three-dimensionally integrated EKE and EAPE associated with cyclonic and anticyclonic vortices, respectively. Throughout the cold season, cyclonic EKE (blue line) and EAPE (red line) are larger than those associated with anticyclonic vortices, presumably because of stronger fluctuations in wind and temperature associated with cyclonic vortices in the lower and mid-troposphere. For cyclonic vortices, EKE and EAPE are nearly constant throughout the cold season, with a subtle peak of total eddy energy (EKE+EAPE; black lines) in early winter (Fig. 9a), which is consistent with the nearly constant cyclonic $V'V'_{300}$ (Fig. 2). Conversely, both the early-winter peak, midwinter suppression and a secondary spring peak are more distinct for anticyclonic EKE and EAPE (Fig. 9b), reflecting the obvious MWM of $V'V'_{300}$ (Fig. 2).

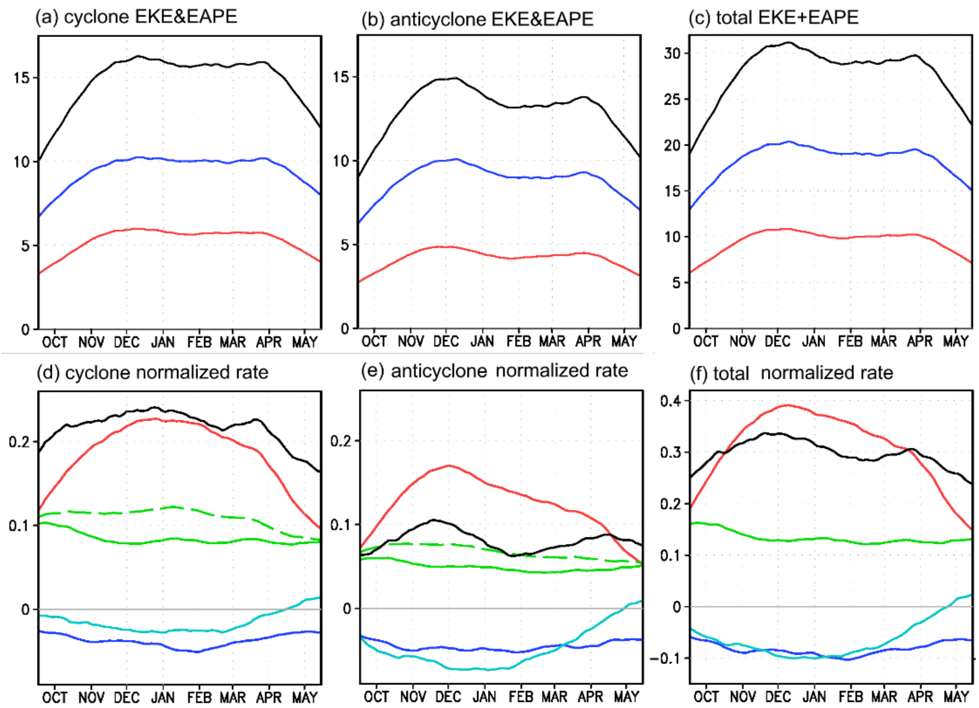

Fig. 9. (a) Climatological-mean seasonal evolution of EKE (blue), EAPE (red), and EKE+EAPE (black) associated only with cyclonic vortices (10^{18}J). All the quantities plotted are integrated three-dimensionally over the North Pacific. A tick mark on the abscissa represents the first day of a given calendar month. (b) Same as in (a), but for anticyclonic vortices. (c) Same as in (a), but for the sum of the cyclonic and anticyclonic contributions. (d-f) Same as in (a-c), respectively, but for "normalized conversion/generation rates" of λ_{CK} (blue), λ_{CP} (red), λ_{CQ} (solid green), λ_{CQ} associated only with precipitation (dashed green), and λ_{EF} (light blue). Black line denotes λ_{Tot} relevant to the budget of EKE+EAPE (viz. CK+CP+CQ+EF). Unit: day^{-1}.

As described in section 2, we calculate the normalized rate ("λ") of each of the energy conversion/generation terms by dividing it by the total energy associated with transient eddies (without separating cyclonic and anticyclonic contributions), to investigate maintenance mechanisms for the NP storm-track activity more quantitatively (Figs. 9d-e). Throughout the cold season, cyclonic vortices tend to be more "energetic" than anticyclonic vortices, with substantially higher net normalized rate (λ_{Tot}; black lines) of energy conversion and generation. Noteworthy, λ_{Tot} for anticyclonic vortices exhibits a well-defined MWM, while the corresponding midwinter reduction for cyclonic vortices is rather modest. This seems consistent with the seasonality of their total energy (Figs. 9a-b).

For both cyclonic and anticyclonic vortices, λ_{CP} (red lines) is much higher than any other conversion/generation rates during the cold seasons. In other words, the baroclinic energy conversion is the most important maintenance mechanism for cyclonic and anticyclonic vortices over the North Pacific, consistent with their baroclinic nature. Interestingly, λ_{CP} for cyclonic vortices is higher but not apparently suppressed in midwinter, while its anticyclonic counterpart peaks in early winter and undergoes more apparent suppression in midwinter. This contrasting seasonality is consistent with the more obvious midwinter suppression in $V'T'_{850}$ for anticyclonic vortices (Fig. 3). The early-winter peak in anticyclonic λ_{CP} is contributed to partly by the early-winter maximum in mid-tropospheric $V'T'$ associated with anticyclonic vortices (Fig. 4). Given that anticyclonic vortices tend to be located near the westerly jet axis compared to cyclonic vortices in the middle and upper troposphere, the more distinct reduction in anticyclonic λ_{CP} from early winter to midwinter than the cyclonic counterpart seems consistent with Hadas and Kaspi (2021).

Compared to λ_{CP}, λ_{CQ} (green lines) is less constructive throughout the winter with no signature of MWM for both cyclonic and anticyclonic vortices. The higher λ_{CQ} associated only with precipitation (green dashed lines) than the net λ_{CQ} (green solid lines) reflects the thermal damping due to eddy heat exchange with the underlying ocean.

For the cyclonic λ_{Tot}, its early-winter peak and subsequent slight decrease into February arise mainly from λ_{CP}, with a slight contribution from λ_{CK} (blue lines), which becomes slightly more destructive into midwinter. The spring recovery of the cyclonic λ_{Tot} is, by contrast, due mainly to λ_{EF} (light blue lines) and additionally to the cyclonic λ_{CK}, which becomes less destructive into spring. For the anticyclonic λ_{Tot}, its marked decrease into midwinter after its early-winter peak is attributable to both λ_{CP} and λ_{EF}, the latter of which becomes more destructive into January. The contribution from λ_{CK} is much more modest. The spring recovery of the anticyclonic λ_{Tot} after its MWM is due primarily to λ_{EF}, which fully offsets the continuous reduction of λ_{CP} into spring. The contribution from λ_{CK} is again much more modest.

As discussed above, λ_{EF} for anticyclonic vortices is most destructive in January. This indicates that anticyclonic vortices contribute to the net outward transport of eddy energy out of the NP domain most effectively in midwinter. As in ONK21, λ_{EF} can be separated into the contributions from energy fluxes passing through the four lateral boundaries of the rectangular domain and further into the contributions from the advective and eddy flux components. For cyclonic vortices (Figs. 10a, c, e), energy fluxes through the western and eastern boundaries, which are mainly due to the advection by climatological-mean flow, largely cancel out each other. The small net outflux in winter arises mainly from eddy energy flux out of the meridional boundaries. The spring increase of the net cyclonic λ_{EF} is attributable mainly to the advective λ_{EF} (Fig. 10c) with an additional contribution from eddy flux (Fig. 10e). Toward spring, the advective energy influx slightly increases, while the advective outflux is reduced. In addition, eddy geopotential fluxes out of the eastern and meridional boundaries decrease into spring.

For anticyclonic vortices (Figs. 10b, d, f), by contrast, energy flux out of the eastern boundary is substantially larger than the influx through the western boundary, leading to the net negative λ_{EF} especially in early and mid-winter. The large energy outflux in midwinter through the eastern boundary is presumably due to the high probability of anticyclonic vortices downstream of the prominent westerly jet core region (Fig. 1b), which may be attributable to the poleward deflection of the jet over the eastern NP. The outward flux by the mean westerlies through the eastern boundary peaks in early winter, when the connection of storm-track activity between the NP and NA is most discernible (not shown). This advective flux accounts for the major fraction of the net outward energy flux in winter. The contribution from eddy geopotential flux to the seasonality of the net anticyclonic λ_{EF} is in the same sense as the advective contribution but only of secondary importance. The smaller anticyclonic λ_{EF} associated with the eddy geopotential flux through the eastern boundary than its cyclonic counterpart, despite the stronger eastward wave-activity flux associated with anticyclonic vortices (Fig. 4), may arise from those terms that are not related to eddy geopotential fluxes (c.f., Takaya and Nakamura 2001). Note that the results regarding λ_{EF} are qualitatively the same if the eastern boundary is placed at a different longitude (e.g., 140°W).

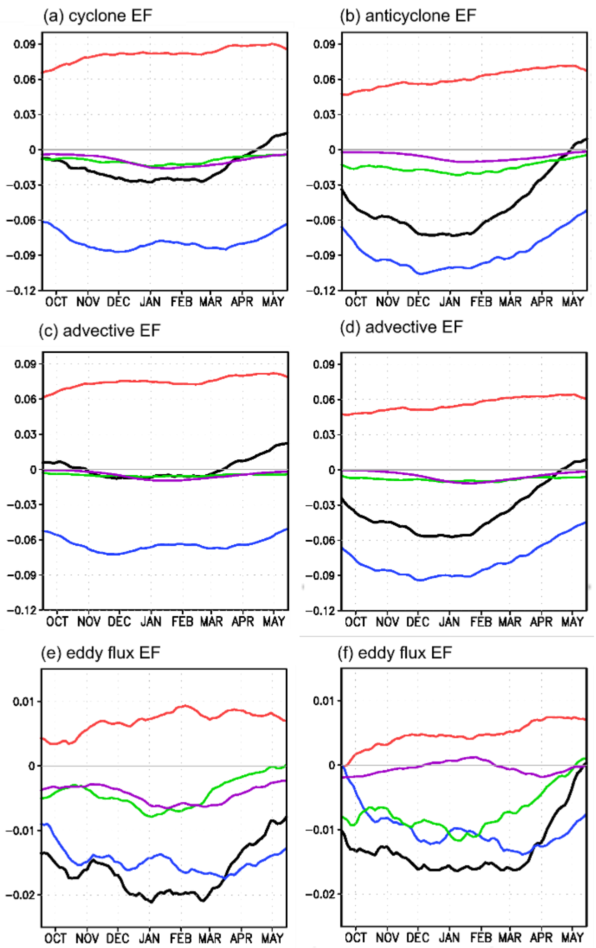

Fig. 10. (a, b) Same as in Figs. 9c-d, respectively, but for the energy fluxes through the western (red), eastern (blue), southern (purple), and northern (green) boundaries of the NP domain. Black line denotes the net total energy flux. Positive (negative) values mean inward (outward) fluxes. (c, d) Same as in (a, b), respectively, but for energy flux associated solely with energy advection by climatological-mean flow. (e, f) Same as in (a, b), respectively, but for energy flux associated solely with eddy geopotential flux.

The above results for transient eddy energetics also include the effect of the seasonality in frequencies of cyclonic and anticyclonic vortices. To verify this effect, we reevaluate energy and conversion/generation efficiencies by normalizing them with the probability of positive/negative curvature averaged within the NP domain [130°−130°W, 20°−65°N], as shown in Fig. 11. As shown in Fig. 1 and Part I, frequency of cyclonic (anticyclonic) vortices basically increases (decreases) in midwinter: more specifically, probability of positive curvature averaged over the reference domain is ~60% in midwinter, while ~50-55% in the shoulder seasons. Although the seasonal evolutions of cyclonic and anticyclonic EKE and

EAPE thus obtained exhibit certain resemblance to those without the normalization by frequency, anticyclonic EKE and EAPE normalized by their frequencies are larger than their cyclonic counterpart (Figs. 11a-b), implying that anticyclonic vortices are not necessarily less energetic than cyclonic vortices. As for the normalized energy conversion/generation rates, the net rate is still higher for cyclonic vortices, owing mainly to the more effective λ_{CP} and less destructive λ_{EF}. With the normalization by frequency, the late-winter minimum of the net normalized rate for cyclonic vortices becomes more distinct. Conversely, the MWM of anticyclonic net normalized rate becomes slightly less discernible. Consequently, the seasonality of the net normalized rates of cyclonic and anticyclonic vortices becomes closer to each other.

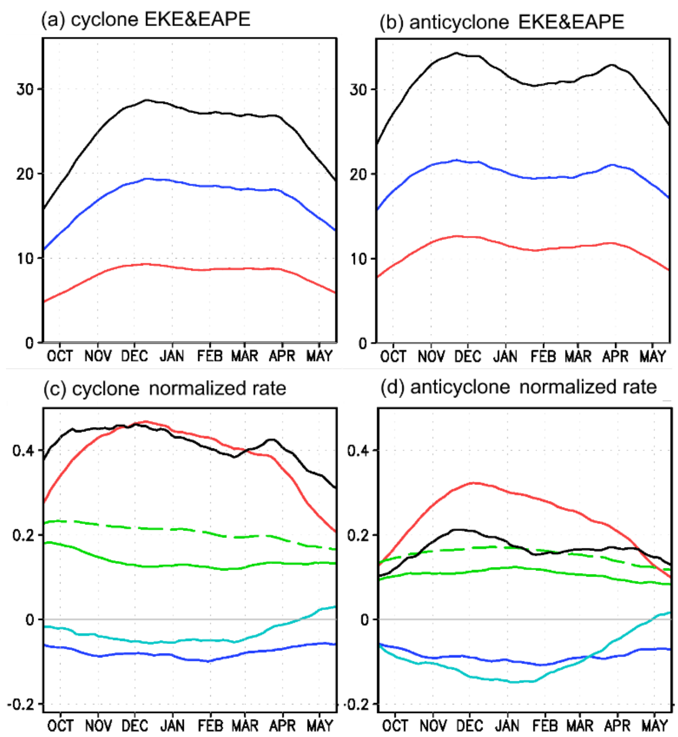

Fig. 11. Same as in Fig. 9, but for the results normalized by frequency of cyclonic and anticyclonic vortices averaged over the North Pacific domain.

Finally, it should be noted that the above results are qualitatively similar with a threshold curvature of 4×10^{-7} m^{-1}, equivalently radius of 2500km.

6. Long-term modulations

In this section, we briefly describe long-term modulations of the contributions to the energetics from cyclone and anticyclone vortices. As in Part I, we divide the full analysis period into the earlier (1958/59−1985/86) and later (1986/87−2016/17) periods, following Nakamura et al. (2002). The result of the energetics for migratory eddies along the NP storm-track separately for the two periods is comparable with ONK22.

In the earlier period, when the MWM of the NP storm-track activity was more distinct, both cyclonic and anticyclonic EKE and EAPE contributed to the more distinct MWM (Figs. 12a, e). In the later period, by contrast, their MWM signatures became less distinct or even almost vanished (Figs. 12b, f), in association with enhanced midwinter EKE and EAPE. This means that both cyclonic and anticyclonic vortices contribute to the long-term modulations of the MWM of the NP storm-track activity as evident in the full Eulerian statistics (ONK22).

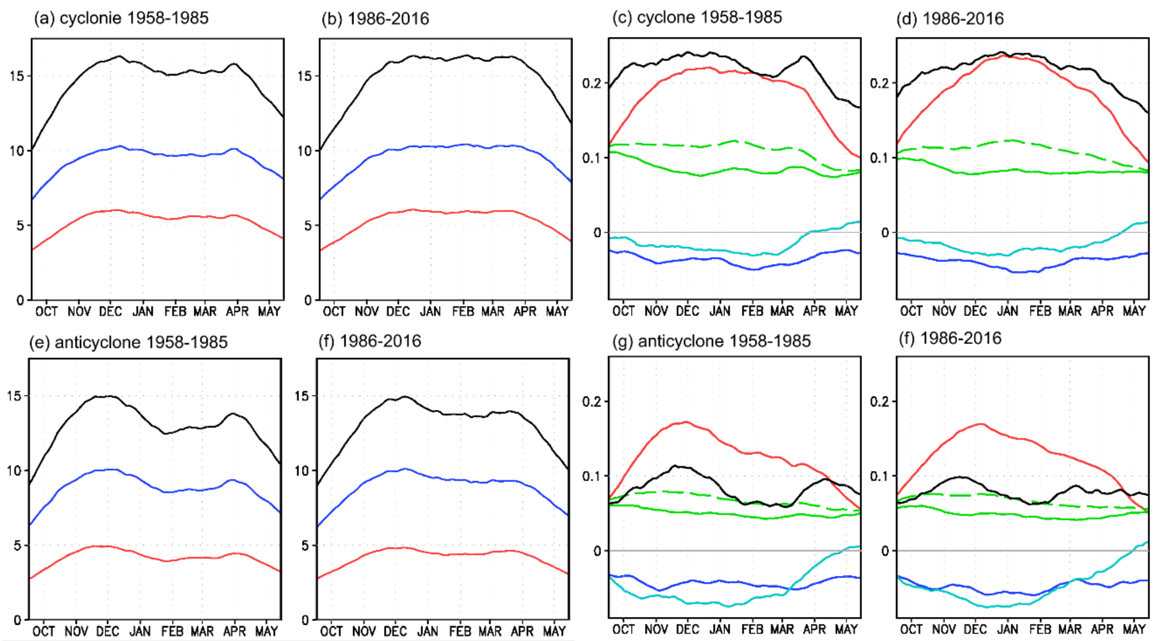

Fig. 12. (a, b) Same as in Fig. 9a, but for the periods of (a) 1958/59−1985/86 and (b) 1986/87−2016/17, respectively. Unit: 10^{18}J. (c, d) Same as in Fig. 9c, but for the periods of (c) 1958/59−1985/86 and (d) 1986/87−2016/17, respectively. Unit: day^{-1}. (e-f) Same as in (a-d), respectively, but for anticyclonic vortices.

As in section 4, we apply the energetic framework separately for the two periods. The midwinter reduction in λ_{Tot} associated with anticyclonic vortices has also been weakened in the later period, though the minimum is still noticeable (Figs. 12g-h). The enhancement of λ_{Tot} by anticyclonic vortices is contributed to by midwinter increase in λ_{CP}, while λ_{EF} becomes more destructive in spring and thus responsible for the reduced spring recovery of λ_{Tot}. The reduced λ_{Tot} in late winter for cyclonic vortices was clearly seen in the earlier period (Fig. 12c), but it has disappeared in the later period (Fig. 12d). This interdecadal enhancement of the late-winter λ_{Tot} is caused by the enhanced λ_{CP} as well as the reduced destructive contribution from λ_{EF}.

Meanwhile, the destructive midwinter λ_{CK} has become more prominent in the later period form both cyclonic and anticyclonic vortices, which is mainly due to its "meridional" component related to $U'V'$ (not shown). This suggests that the lateral shear of the NP westerly jet, which is assumed to be essential in the "barotropic governor" mechanism, is not necessarily relevant to the interdecadal enhancement of the midwinter NP storm-track activity for both cyclonic and anticyclonic vortices.

7. Summary and Discussions

As Part II of the paired papers, the present study has investigated the detailed seasonal evolution of contributions from cyclonic and anticyclonic vortices to Eulerian eddy statistics, eddy feedback forcing onto the climatological-mean westerly jet, and energetics associated with the NP storm-track. This has been achieved by combining the framework for the comprehensive energetics that is independent of eddy amplitude and the method for evaluating separate contributions from cyclonic and anticyclonic vortices to Eulerian eddy statistics through identifying three-dimensional domains of cyclonic and anticyclonic vortices based on local curvature. This "hybrid perspective" effectively illustrates the seasonal evolution of the contributions from cyclonic and anticyclonic vortices to Eulerian eddy statistics and atmospheric energetics.

The key finding of this study is that the MWM of the net energy conversion/generation rate normalized by the eddy total energy (λ_{Tot}) over the entire NP is more distinct for anticyclonic vortices than for cyclonic vortices. Together with Part I, the present study is the first to reveal the primal importance of migratory anticyclones for the MWM of the NP storm-track activity in a quantitative fashion. Given their broader and drier property compared to cyclones, the conclusion is compatible with the fact that the MWM of the NP storm-track activity has been reproduced even in coarse-resolution GCMs (Christoph et al. 1997; Zhang and Held 1997). We posit the viewpoint of considering both migratory cyclones and anticyclones for the storm-track dynamics, where the latter has been long overlooked.

As mentioned by Wallace et al. (1988), the term *storm-track* used by Blackmon et al. (1977) implies that Eulerian eddy statistics are exclusively associated with cyclone tracks and thus anticyclone tracks are somehow irrelevant. Wallace et al. (1988) pointed out, however, that it is not necessarily the case, because the Eulerian eddy statistics does not imply any sense of polarity. The "hybrid perspective" of storm-track dynamics postulated in this study provides an answer to the long-standing question in a quantitative manner. Specifically, cyclonic vortices are found to contribute predominantly to $V'T'_{850}$ as a typical measure of lower-tropospheric "storm-track" activity, whereas $V'V'_{300}$ as a typical measure of upper-tropospheric "storm-track" activity includes a greater contribution from anticyclonic vortices.

The present study also provides some insights that complement the results based on the detailed energetics with the full Eulerian statistics by ONK22. They found that the higher mid- to upper-tropospheric $V'-T'$ correlation and associated larger $V'T'$ along the NP storm-track in early winter partly contribute to the early-winter peak in λ_{CP}. The present study has revealed that the high $V'-T'$ correlation is associated mainly with anticyclonic vortices, although detailed mechanisms remain unsolved. Additionally, ONK22 pointed out that their result about the contribution from $U'T'$ to *CP* does not seem consistent with Schemm and Rivière (2019), who showed the angle between the vectors of background baroclinicity gradient and eddy heat transport is maximized in midwinter over the western NP, leading to the MWM of the baroclinic energy conversion (*CP*). However, the sign of zonal eddy heat flux is opposite between the upper and lower troposphere (ONK22). The present study has found that a midwinter maximum of positive $U'T'$ below the jet core and another maximum of lower-tropospheric negative $U'T'$ north of ~40°N are distinct particularly for anticyclonic and cyclonic vortices, respectively (not shown). The negative lower-tropospheric $U'-T'$ correlation is more distinct in midwinter for both cyclonic and anticyclonic vortices, suggesting that they tend to tilt equatorward with height, presumably reflecting upper-tropospheric eddies trapped into the equatorward-shifted westerly jet, as suggested by some earlier studies (Nakamura and Sampe 2002; Hadas and Kaspi 2021). Nevertheless, the cyclonic contribution is dominant for the negative lower-tropospheric $U'-T'$ correlation, owing to their higher probability than that of anticyclonic vortices north of ~40°N. Indeed, slight positive midwinter λ_{CP} associated with $U'T'$ pointed out by ONK22 is mostly due to cyclonic vortices (not shown), which is supportive of the above discussion. In other words, the tendency of midwinter NP cyclones to be more equatorward-tilted with height acts to attenuate the MWM of the NP storm-track activity, although its contribution is overwhelmed by *CP* associated with $V'T'$.

Considering that *CP* is the most important process for the maintenance of both cyclonic and anticyclonic vortices, it is of interest what brings the seasonality of cyclonic and anticyclonic contributions to $V'T'_{850}$. Figure 13 shows the decomposed contributions of $V'V'_{850}$, $T'T'_{850}$, and $V'-T'$ correlation at 850-hPa to $V'T'_{850}$ $\left(=\sqrt{V'V'_{850}\cdot T'T'_{850}}\cdot \mathrm{Corr}(V'_{850}, T'_{850})\right)$. Consistent with Fig. 3, the MWM of $V'T'_{850}$ is more distinct for anticyclonic vortices (Fig. 13a), arising from all the contributions from velocity and temperature fluctuations, as well as the $V'-T'$ correlation. In addition, cyclonic $T'T'_{850}$ also exhibits a clear MWM. The seasonal evolution of the cyclonic and anticyclonic $V'-T'$ correlation coefficients implies that cyclonic vortices tend to be slightly more baroclinic in the lower troposphere, with highest $V'-T'$ correlation in midwinter.

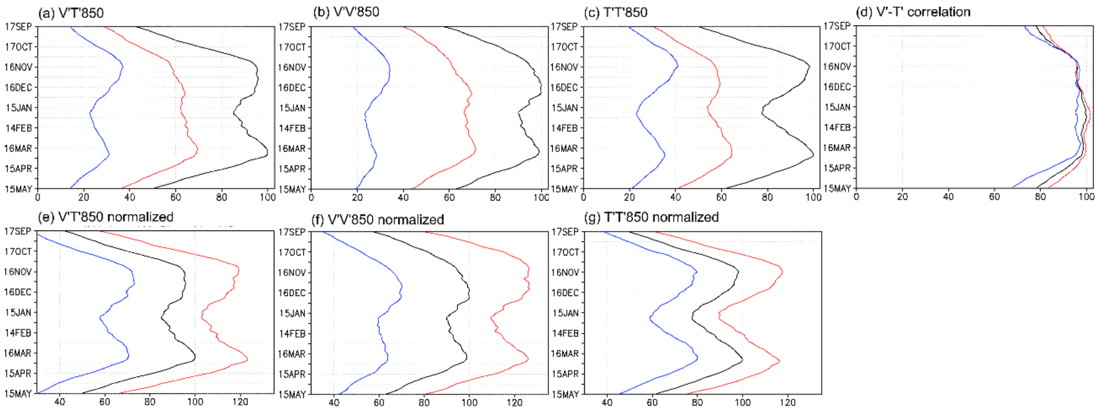

Fig. 13. (a) Climatological-mean $V'T'_{850}$ averaged longitudinally for 150°−180°E. All the quantities plotted are meridionally-averaged within 9 grids whose center is at its maximum in 25°–55°N of the total climatological-mean $V'T'_{850}$ at each longitude. Red, blue, and black lines indicate $V'T'_{850}$ by cyclonic and anticyclonic domains, and the total climatological mean, respectively. The values are normalized so that the maximum of the total climatological-mean is set to 100%. (b-d) Same as in (a), but for (b) $V'V'_{850}$, (c) $T'T'_{850}$, and (d) V'–T' correlation at 850-hPa averaged for 150°-180°E. Again, those quantities are averaged around the axis of the total climatological-mean $V'T'_{850}$ at each longitude. (e-g) Same as in (a-c), respectively, but for quantities normalized by probability of cyclonic or anticyclonic vortices averaged meridionally around the $V'T'_{850}$ axis.

Those contributions to $V'T'_{850}$ are also influenced by the seasonal evolution of lower-tropospheric probability of cyclonic and anticyclonic vortices, in which cyclonic vortices are more frequent along the NP storm-track axis as seen in Figs. 1d-f. We further examine the seasonality of the cyclonic and anticyclonic $V'T'_{850}$, $V'V'_{850}$, and $T'T'_{850}$ by normalizing them separately with the probabilities of cyclonic and anticyclonic vortices averaged meridionally around the $V'T'_{850}$ axis. The seasonality shown in Figs. 13e-g, which is thus independent of that of the probability, indicates that those eddy statistics related to cyclonic vortices also substantially decreased in magnitude in midwinter, which is consistent with Hoskins and Hodges (2019). This is indicative of the primal importance of the different seasonality of probability between cyclonic and anticyclonic vortices. Additionally, for both cyclonic and anticyclonic vortices, $T'T'_{850}$ is more important for the MWM of $V'T'_{850}$.

On the basis of the results obtained in this paper and Part I, Fig. 14 schematically illustrates climatological-mean evolution of the NP storm-track activity during the cold season. In comparison with the shoulder seasons, the midwinter situation is characterized by the following factors:

- Higher mid-tropospheric static stability over the Japan Sea. This is attributable partly to the stronger Siberian High and the associated cold low-level monsoonal airflow. The higher static stability retards the vertical connection of upper-tropospheric eddies with lower-tropospheric disturbances, which leads to less frequent formation of surface migratory anticyclones over the Japan Sea.
- Less frequent upper-tropospheric anticyclonic vortices over the Japan Sea (Part I). In sharp contrast, cyclonic vortices become more frequent from early- to mid-winter around ~40°N.
- Enhanced energy outflux downstream from the eastern NP associated mainly with anticyclonic vortices. This is presumably due to their high probability downstream of the jet core region. It may be explained by the poleward deflection of the midwinter westerly jet, on the equatorward flank of which "trough thinning and broadening" mechanism (Thorncroft et al. 1993) may be favorable for anticyclonic vortices. The poleward jet deflection may be a manifestation of seasonally intensified planetary waves (Wang and Ting 1999). Rodwell and Hoskins (2001) stressed the importance of the interaction between the zonal-mean flow and large-scale mountains for wintertime subtropical circulation, especially the equivalent-barotropic stationary anticyclone west of high mountains, while Orlanski (1998) argued that eddy feedback forcing has a similar effect. Indeed, our analysis indicates that transient eddy components, especially those associated with anticyclonic vortices, act to shift the jet axis poleward over the eastern NP. Another possible explanation is that migratory anticyclones, by nature, tend to propagate farther downstream compared to cyclones,

given the poleward-propagating tendency of cyclones away from the jet related to diabatic heating (Tamarin and Kaspi 2016). The relationship between the poleward deflection of the jet and the high probability of anticyclonic vortices over the eastern NP under the eddy-mean flow interaction is to be further examined.

- Weaker background baroclinicity for surface cyclones propagating into the quasi-stationary AL. This is due to their greater distance from the baroclinic zone owing to the equatorward displacement and narrowing of the midwinter westerly jet.

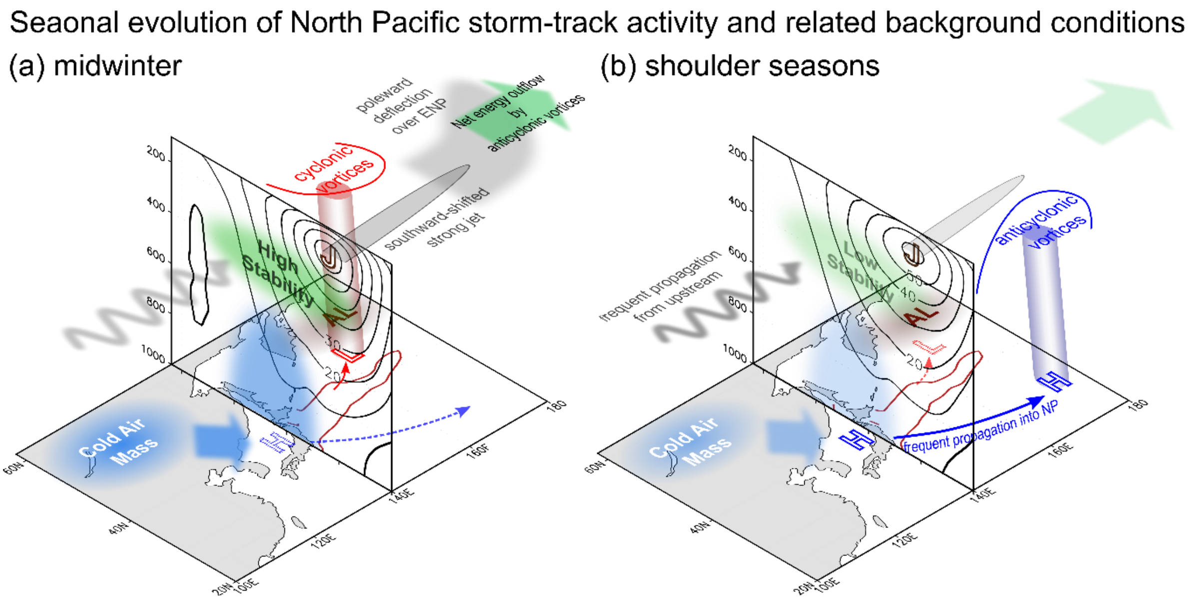

Fig. 14. Schematic diagrams of climatological-mean situations in (a) midwinter and (b) shoulder seasons. Black contours on vertical sections indicate zonally-averaged climatological-mean westerly wind speed (m/s) for 130°−140°E on (a) 24Jan and (b) 19Mar.

The activity of cyclonic and anticyclonic vortices may be related to cyclonic/anticyclonic Rossby wave breaking named LC2 and LC1, respectively (Thorncroft et al. 1993). It is suggested that LC1 wave breaking acts to draw westerly momentum from an upper-tropospheric subtropical jet into a midlatitude eddy-driven jet. By contrast, LC2 is likely to occur under the cyclonic shear of a westerly jet, leading to the development of a cyclonic vortex on the poleward flank of the jet, as observed in the midlatitude western NP. The dominance of LC1 or LC2 in a numerical model used by Thorncroft et al. (1993) is sensitive to a parameter chosen for the structure of an initial westerly distribution (Hartmann and Zuercher 1998). Nevertheless, the results by Thorncroft et al. (1993) seem consistent with the probability distributions of cyclonic and anticyclonic vortices obtained through our vorticity identification based on local curvature (Fig. 1). Moreover, based on a dry idealized model, Garfinkel and Waugh (2014) suggested that LC1 frequency tends to decrease on the equatorward flank of a westerly jet when shifted equatorward, which is compatible with the seasonal evolution of the NP storm-track. A linearized barotropic model experimented by Lorenz (2014) indicated that the stronger a westerly jet, the more poleward-propagating Rossby waves tend to be reflected around its poleward fringe (i.e., adjacent reflecting latitude), leading to an anomalous poleward flux of westerly momentum associated with equatorward-propagating waves after their reflection.

The results about the atmospheric energetics obtained in the present study can be regarded as a decomposition of the normalized energy conversion/generation rates obtained in ONK22 into cyclonic and anticyclonic contributions. We have confirmed that qualitatively similar results are obtained on the eddy energetics with a non-zero threshold of curvature. The present study provides a new perspective for the MWM of the NP storm-track activity by demonstrating the importance of both anticyclones and cyclones in the investigation of storm-track dynamics. There remains, however, a question to be answered: *why do the two contrasting seasonal evolutions of the activities of cyclonic and anticyclonic vortices lead to the MWM as their net effect?* It can be rephrased from the viewpoint of decomposed energetics: is there any necessity for their net contribution to decrease in the presence of an equatorward-shifted or narrow westerly jet with excessive intensity? Expanding our analysis by including a viewpoint from Rossby wave breaking will certainly be informative. It will be also informative to address the fundamental question by, for example, applying our framework to idealized experiments in which a jet stream can be artificially manipulated. The incorporation of energy exchange terms between cyclonic and anticyclonic vortices into the framework proposed in this study is also needed as an important future topic.

While some of the factors pointed out in this study are inherent to the geographical characteristics around the NP, which may be viewed as local effects, the present study can also fit with Yuval et al. (2018) and Novak et al. (2020), who argued that the MWM of the storm-track activity can be reproduced in idealized GCM experiments with zonally-symmetric lower-boundary conditions. Although the excessively strong Pacific jet owes its existence to such local effects as the climatologically deep East Asian trough, a stronger westerly jet, even if zonally uniform, may induce a higher probability of anticyclonic wave breaking on its equatorward flank, as suggested by previous studies.

The relationship between the results obtained in the present study and Part I needs to be further studied. This is because this paper explores contributions from three-dimensional cyclonic and anticyclonic vortices to Eulerian eddy statistics, whereas Part I focuses on centers of surface migratory disturbances, in which vortices without any distinct surface extrema have been excluded. The seasonality of composited structure of surface anticyclones should be investigated in the future. Additionally, the air-sea interaction associated with cyclones and anticyclones, especially over the North Pacific oceanic frontal zones, needs to be examined.

Finally, the analyses performed in this study are applicable to storm-tracks over other ocean basins. Comparison between the NP and NA storm-tracks within the framework of this study would be beneficial for further deepening of our understanding of storm-track dynamics and the MWM in storm-track activity. Our preliminary result suggests that, unlike the NP storm-track, there is no MWM in λ_{Tot} associated with anticyclonic vortices over the NA. A brief investigation of the long-term modulations of the MWM of the NP storm-track activity in this study should be complemented by a more detailed analysis in future. Interannual variability of the storm-track activity is also in our future scope. Furthermore, the framework of the present study may also be applicable to storm-tracks under the past and future climate, including the reduced storm-track activity during the last glacial maximum (Li and Battisti 2008).

Acknowledgments.

This study is supported in part by the Japanese Ministry of Education, Culture, Sports, Science and Technology (MEXT) through the Arctic Challenge for Sustainability (ArCS-II), by the Japan Science and Technology Agency through COI-NEXT JPMJPF2013, by the Environmental Restoration and Conservation Agency of Japan through Environment Research and Technology Development Fund JPMEERF20222002, and by the Japan Society for the Promotion of Science (JSPS) through Grants-in-Aid for Scientific Research 19H05702 (on Innovative Areas 6102), 20H01970, 22H01292 and 22K14097. It is also supported by JSPS-ISF Joint Research Project (JPJSBP120218403). Y.K. acknowledges support from the JSPS Invitational Fellowship for Research in Japan that supported a sabbatical at the University of Tokyo and ignited this collaboration, for support from the

Research Center for Advanced Technology and Science at the University of Tokyo and the Israeli Science Foundation (grant 996/20).

Data Availability Statement.

The JRA-55 atmospheric reanalysis is available online from the Japan Meteorological Agency at https://jra.kishou.go.jp/JRA-55/index_en.html as cited in Kobayashi et al. (2015) and Harada et al. (2016).

REFERENCES

Afargan, H., and Y. Kaspi, 2017: A midwinter minimum in North Atlantic storm track intensity in years of a strong jet. Geophys. Res. Lett., 44(24), 12–511.

Barnes, E. A., and D. L. Hartmann, 2011: Rossby wave scales, propagation, and the variability of eddy-driven jets. J. Atmos. Sci., 68(12), 2893-2908.

Barnes, E. A., and D. L. Hartmann, 2012: Detection of Rossby wave breaking and its response to shifts of the midlatitude jet with climate change. J. Geophys. Res.: Atmos., 117(D9).

Barnes, E. A., and L. Polvani, 2013: Response of the midlatitude jets, and of their variability, to increased greenhouse gases in the CMIP5 models. J. Climate, 26(18), 7117-7135.

Blackmon, M. L., 1976: A climatological spectral study of the 500 mb geopotential height of the Northern Hemisphere. J. Atmos. Sci., 33(8), 1607–1623.

Blackmon, M. L., J. M. Wallace, N. C. Lau, and S. L. Mullen, 1977: An observational study of the Northern Hemisphere wintertime circulation. J. Atmos. Sci., 34(7), 1040–1053.

Chang, E. K., 1993: Downstream development of baroclinic waves as inferred from regression analysis. J. Atmos. Sci., 50(13), 2038–2053.

Chang, E. K., 2001: GCM and observational diagnoses of the seasonal and interannual variations of the Pacific storm track during the cool season. J. Atmos. Sci., 58(13), 1784–1800.

Chang, E. K., S. Lee, and K. L. Swanson, 2002: Storm track dynamics. J. Climate, 15(16), 2163–2183.

Chang, E. K., and S. Song, 2006: The seasonal cycles in the distribution of precipitation around cyclones in the western North Pacific and Atlantic. J. Atmos. Sci., 63(3), 815–839.

Chang, E. K., and Y. Guo, 2012: Is Pacific storm-track activity correlated with the strength of upstream wave seeding?, J. Climate, 25(17), 5768–5776.

Christoph, M., U. Ulbrich, and P. Speth, 1997: Midwinter suppression of Northern Hemisphere storm track activity in the real atmosphere and in GCM experiments. J. Atmos. Sci., 54(12), 1589–1599.

Deng, Y., and M. Mak, 2005: An idealized model study relevant to the dynamics of the midwinter minimum of the Pacific storm track. J. Atmos. Sci., 62(4), 1209–1225.

Deng, Y., and M. Mak, 2006: Nature of the differences in the intraseasonal variability of the Pacific and Atlantic storm tracks: A diagnostic study. J. Atmos. Sci., 63(10), 2602–2615.

Eady, E. T., 1949: Long waves and cyclone waves. Tellus, 1(3), 33–52.

Garfinkel, C. I., and D. W. Waugh, 2014: Tropospheric Rossby wave breaking and variability of the latitude of the eddy-driven jet. J. Climate, 27(18), 7069-7085.

Goldman, R., 2005: Curvature formulas for implicit curves and surfaces. Comput. Aided Geom. Des., 22(7), 632-658.

Hadas, O., and Y. Kaspi, 2021: Suppression of baroclinic eddies by strong jets. J. Atmos. Sci., in press.

Harada, Y., H. Kamahori, C. Kobayashi, H. Endo, S. Kobayashi, Y. Ota, H. Onoda, K. Onogi, K. Miyaoka, and K. Takahashi, 2016: The JRA-55 Reanalysis: Representation of atmospheric circulation and climate variability, J. Meteor. Soc. Japan, 94, 269–302.

Harnik, N., and E. K. Chang, 2004: The effects of variations in jet width on the growth of baroclinic waves: Implications for midwinter Pacific storm track variability. J. Atmos. Sci., 61(1), 23–40.

Hartmann, D. L., and P. Zuercher, 1998: Response of baroclinic life cycles to barotropic shear. J. Atmos. Sci., 55(3), 297-313.

Hoskins, B. J., and K. I. Hodges, 2019: The annual cycle of Northern Hemisphere storm tracks. Part II: Regional detail. J. Climate, 32(6), 1761-1775.

Hotta, D., and H. Nakamura, 2011: On the significance of the sensible heat supply from the ocean in the maintenance of the mean baroclinicity along storm tracks. J. Climate, 24(13), 3377–3401.

James, I. N., 1987: Suppression of baroclinic instability in horizontally sheared flows. J. Atmos. Sci., 44(24), 3710–3720.

Klinker, E., and P. D. Sardeshmukh, 1992: The diagnosis of mechanical dissipation in the atmosphere from large-scale balance requirements. J. Atmos. Sci., 49(7), 608–627.

Kobayashi, S., Y. Ota, Y. Harada, A. Ebita, M. Moriya, H. Onoda, K. Onogi, H. Kamahori, C. Kobayashi, H. Endo, K. Miyaoka, and K. Takahashi, 2015: The JRA-55 Reanalysis: General specifications and basic characteristics. J. Meteor. Soc. Japan, 93, 5–48.

Kuwano-Yoshida, A., S. Okajima, and H. Nakamura, 2021: Rapid increase of explosive cyclone activity over the midwinter North Pacific in the late 1980s. J. Climate, 35(3), 1113-1133.

Lachmy, O., and N. Harnik, 2014: The transition to a subtropical jet regime and its maintenance. J. Atmos. Sci., 71(4), 1389–1409.

Lachmy, O., and N. Harnik, 2016: Wave and jet maintenance in different flow regimes. J. Atmos. Sci., 73(6), 2465–2484.

Landsberg, H., J. M. Mitchell Jr, and H. Crutcher, 1959: Power Spectrum Analysis of Climatological Data for Woodstock College, Maryland. Mon. Wea. Rev., 87(8), 283-298.

Lau, N. C., and E. O. Holopainen, 1984: Transient eddy forcing of the time-mean flow as identified by geopotential tendencies. J. Atmos. Sci., 41(3), 313-328.

Lau, N. C., and M. J. Nath, 1991: Variability of the baroclinic and barotropic transient eddy forcing associated with monthly changes in the midlatitude storm tracks. J. Atmos. Sci., 48(24), 2589–2613.

Lee, S., and H. K. Kim, 2003: The dynamical relationship between subtropical and eddy-driven jets. J. Atmos. Sci., 60(12), 1490–1503.

Lee, S. S., J. Y. Lee, K. J. Ha, B. Wang, A. Kitoh, Y. Kajikawa, and M. Abe, 2013: Role of the Tibetan Plateau on the annual variation of mean atmospheric circulation and storm-track activity. J. Climate, 26(14), 5270–5286.

Lefevre, R. J., and J. W. Nielsen-Gammon, 1995: An objective climatology of mobile troughs in the Northern Hemisphere. Tellus A, 47(5), 638-655.

Li, C., and D. S. Battisti, 2008: Reduced Atlantic storminess during Last Glacial Maximum: Evidence from a coupled climate model. J. Climate, 21(14), 3561-3579.

Lorenz, E. N., 1955: Available potential energy and the maintenance of the general circulation. Tellus, 7(2), 157-167.

Lorenz, D. J., 2014: Understanding midlatitude jet variability and change using Rossby wave chromatography: Poleward-shifted jets in response to external forcing. J. Atmos. Sci., 71(7), 2370-2389.

Madonna, E., C. Li, and J. J. Wettstein, 2019: Suppressed eddy driving during southward excursions of the North Atlantic jet on synoptic to seasonal time scales. Atmos. Sci. Lett., 20(9), e937.

Mak, M., 1982: On moist quasi-geostrophic baroclinic instability. J. Atmos. Sci., 39(9), 2028-2037.

Mak, M., 1994: Cyclogenesis in a conditionally unstable moist baroclinic atmosphere. Tellus A, 46: 14-33.

Martineau, P., H. Nakamura, Y. Kosaka, and A. Yamamoto, 2020: Importance of a vertically tilting structure for energizing the North Atlantic Oscillation. Sci. Rep., 10(1), 1-10.

Nakamura, H., 1992: Midwinter suppression of baroclinic wave activity in the Pacific. J. Atmos. Sci., 49(17), 1629–1642.

Nakamura, H., and T. Sampe, 2002: Trapping of synoptic-scale disturbances into the North-Pacific subtropical jet core in midwinter. Geophys. Res. Lett., 29(16), 8–1.

Nakamura, H., T. Izumi, and T. Sampe, 2002: Interannual and decadal modulations recently observed in the Pacific storm track activity and East Asian winter monsoon. J. Climate, 15(14), 1855–1874.

Nakamura, H., T. Sampe, Y. Tanimoto, and A. Shimpo, 2004: Observed associations among storm tracks, jet streams, and midlatitude oceanic fronts. Earth Climate: The Ocean–Atmosphere Interaction, Geophys. Monogr., 147, Amer. Geophys. Union, 329–345.

Nakamura, H., and A. Shimpo, 2004: Seasonal variations in the Southern Hemisphere storm tracks and jet streams as revealed in a reanalysis dataset. J. Climate, 17(9), 1828-1844.

Novak, L., T. Schneider, and F. Ait-Chaalal, 2020: Midwinter suppression of storm tracks in an idealized zonally symmetric setting. J. Atmos. Sci., 77(1), 297–313.

Okajima, S., H. Nakamura, and Y. Kaspi, 2021: Cyclonic and anticyclonic contributions to atmospheric energetics. Sci. Rep., 11(1), 1-10.

Okajima, S., H. Nakamura, and Y. Kaspi, 2022a: Energetics of transient eddies related to the midwinter minimum of the North Pacific storm-track activity. J. Climate, 35(4), 1137-1156.

Okajima, S., H. Nakamura, and Y. Kaspi, 2022b: Distinct roles of cyclones and anticyclones in the midwinter minimum of the North Pacific storm-track activity. Part I: Lagrangian perspective. J. Climate, submitted.

Orlanski, I., 1998: Poleward deflection of storm tracks. J. Atmos. Sci., 55(16), 2577-2602.

Orlanski, I. and J. Katzfey, 1991: The life cycle of a cyclone wave in the Southern Hemisphere. Part I: Eddy energy budget. J. Atmos. Sci., 48(17), 1972–1998.

Park, H. S., J. C. Chiang, and S. W. Son, 2010: The role of the central Asian mountains on the midwinter suppression of North Pacific storminess. J. Atmos. Sci., 67(11), 3706–3720.

Penny, S., G. H. Roe, and D. S. Battisti, 2010: The source of the midwinter suppression in storminess over the North Pacific. J. Climate, 23(3), 634–648.

Penny, S. M., D. S. Battisti, and G. H. Roe, 2013: Examining mechanisms of variability within the Pacific storm track: Upstream seeding and jet-core strength. J. Climate, 26(14), 5242–5259.

Rivière, G., and A. Joly, 2006: Role of the Low-Frequency Deformation Field on the Explosive Growth of Extratropical Cyclones at the Jet Exit. Part I: Barotropic Critical Region, J. Atmos. Sci., 63(8), 1965-1981.

Rivière, G., S. Berthou, G. Lapeyre, and M. Kageyama, 2018: On the Reduced North Atlantic Storminess during the Last Glacial Period: The Role of Topography in Shaping Synoptic Eddies, J. Climate, 31(4), 1637-1652.

Robert, L., G. Rivière, and F. Codron, 2017: Positive and negative eddy feedbacks acting on midlatitude jet variability in a three-level quasigeostrophic model. J. Atmos. Sci., 74(5), 1635–1649.

Rodwell, M. J., and B. J. Hoskins, 2001: Subtropical anticyclones and summer monsoons. J. Climate, 14(15), 3192-3211.

Schemm, S., and T. Schneider, 2018: Eddy lifetime, number, and diffusivity and the suppression of eddy kinetic energy in midwinter. J. Climate, 31(14), 5649-5665.

Schemm, S., and G. Rivière, 2019: On the Efficiency of Baroclinic Eddy Growth and how it Reduces the North Pacific Storm Track Intensity in Midwinter. J. Climate, 32(23), 8373–8398.

Schemm, S., S. Rüdisühli, and M. Sprenger, 2020: The life cycle of upper-level troughs and ridges: a novel detection method, climatologies and Lagrangian characteristics. Wea. Clim. Dyn., 1(2), 459-479.

Schemm, S., H. Wernli, and H. Binder, 2021: The storm-track suppression over the western North Pacific from a cyclone life-cycle perspective, Wea. Clim. Dyn., 2, 55-69.

Takaya, K., and H. Nakamura, 2001: A formulation of a phase-independent wave-activity flux for stationary and migratory quasigeostrophic eddies on a zonally varying basic flow. J. Atmos. Sci., 58, 608–627.

Tamarin, T., and Y. Kaspi, 2016: The poleward motion of extratropical cyclones from a potential vorticity tendency analysis. J. Atmos. Sci., 73(4), 1687-1707.

Thorncroft, C. D., B. J. Hoskins, and M. E. McIntyre, 1993: Two paradigms of baroclinic-wave life-cycle behaviour. Quart. J. Roy. Meteor. Soc., 119(509), 17-55.

Trenberth, K. E., 1986: An assessment of the impact of transient eddies on the zonal flow during a blocking episode using localized Eliassen-Palm flux diagnostics. J. Atmos. Sci., 43, 2070–2087.

Wallace, J. M., G. H. Lim, and M. L. Blackmon, 1988: Relationship between cyclone tracks, anticyclone tracks and baroclinic waveguides. J. Atmos. Sci., 45, 439–462.

Wang, H., and M. Ting, 1999: Seasonal cycle of the climatological stationary waves in the NCEP–NCAR reanalysis. J. Atmos. Sci., 56(22), 3892-3919.

Whitaker, J. S., and P. D. Sardeshmukh, 1998: A linear theory of extratropical synoptic eddy statistics. J. Atmos. Sci., 55(2), 237–258.

Yuval, J., and Y. Kaspi, 2018: Eddy sensitivity to jet characteristics. J. Atmos. Sci., 75(5), 1371–1383.

Yuval, J., H. Afargan, and Y. Kaspi, 2018: The relation between the seasonal changes in jet characteristics and the Pacific Midwinter Minimum in eddy activity. Geophys. Res. Lett., 45(18), 9995–10002.

Zhao, Y., and X. S. Liang, 2019: Causes and underlying dynamic processes of the mid-winter suppression in the North Pacific storm track. Sci. China Earth Sci., 62(5), 872–890.

Zhang, Y., and I. M. Held, 1999: A linear stochastic model of a GCM's midlatitude storm tracks. J. Atmos. Sci., 56(19), 3416–3435.